

Mitigating Motion Sickness in Automated Vehicles With Frequency-Shaping Approach to Motion Planning

Daofei Li and Jiankan Hu

Abstract—With automated driving, human drivers have been partially, and in the future will be fully, relieved from driving tasks, and it becomes more important to mitigate car-sickness in self-driving vehicles. Previous research on reducing motion sickness mostly focus on improving the cockpit environment through human factors engineering, while few efforts have been made through vehicle motion optimization, especially from the view of vehicle longitudinal and lateral accelerations. To this end, we propose a new conception to settle car-sickness issues in motion planning rather than in motion control, i.e., to first plan a desired set of vehicle motion less likely to cause car-sickness and then to track the desired motion. We develop a novel motion planning algorithm via frequency shaping approach, which incorporates the essential mechanism of car-sickness. Simulation and experiment results indicate that the proposed approach can reduce motion sickness dose value (MSDV) by 21 % and 37 %, respectively, comparing with the polynomial-based planning algorithm that optimizes acceleration and jerk magnitudes.

Index Terms—Motion sickness, motion planning, frequency shaping, automated vehicle, ride comfort.

I. INTRODUCTION

THE rapid development of autonomous driving calls for new ways to improve vehicle ride comfort, especially when considering the role change of human driver in manually driven vehicles to a passenger “free to do anything but driving” in future highly-automated vehicles. Although being relieved from busy “driving tasks,” especially in crowded urban traffic, will greatly reduce the human workload, the change of role to “passenger” might bring up some unnecessary ride comfort challenges, especially for those vulnerable to motion sickness.

Motion sickness is a problem maybe as old as the locomotion itself. If considering only those literature related to automated vehicles, several methods have been proposed to mitigate passenger motion sickness. For example, Salter *et al.* find that rear-facing seats are not suggested in automated vehicles [1],

and Miksch *et al.* propose a solution to motion sickness by using front road view as the screen background of passengers’ reading material [2]. Through optimizing the cockpit environment, these methods are useful in reducing motion sickness, and can be also realized in traditional human-driven vehicles. However, for automated vehicles these methods have not fully utilized the advantages of driving automation, especially via motion planning and control.

Kuiper *et al.* [3] compare the influences of predictable and unpredictable motion stimuli on motion sickness and conclude that the unpredictable motion is more provocative. An audio cue is also designed to inform the up-coming motion, which can mitigate motion sickness [4]. It should be noted that in an automated vehicle, the up-coming motion can be easily obtained from the corresponding automated algorithms, and this kind of informative cues, via audio, vision or vibration, can then be conveniently applied. It is practical, but when the motion stimuli from the vehicle are severe, this approach may reach limits of beneficial effects.

The cause of motion sickness is motion itself, if forgiving some passengers’ own susceptibility to motion sickness. Our daily experiences of ground transportation also show that there are some certain driving styles making passengers sick but others not, even if driving the same car on the same path. With the introduction of automated driving, vehicle motion can be almost fully controlled. Briefly speaking, there are usually five basic modules in automated driving, i.e., perception, decision, planning, control, and action. The perception module helps the vehicle “see” the environment, the decision module decides speed and direction to go, and the planning module schedules a path and a velocity profile. To follow the path and the velocity profile, the control module computes appropriate operational inputs, including steering, acceleration and braking, to be finally implemented in the actuators of the action module. Given road traffic conditions and vehicle actuator capability limits, it is mainly planning and control modules that determine the movement of the vehicle.

Knowing that to optimize vehicle motion is the key, motion planning and control should be specially designed considering motion sickness, in addition to driving safety. On one hand, several control methods have been proposed for pleasant vehicle motion. Note that active or semi-active suspensions have been widely adopted in many mid- to high-end vehicles, but most of suspension technologies are for vehicle ride improvement

Manuscript received April 3, 2021; accepted July 25, 2021. Date of publication July 30, 2021; date of current version August 17, 2021. This letter was recommended for publication by Associate Editor A. Pierson and Editor S. J. Guy upon evaluation of the reviewers’ comments. This work was supported in part by the Ningbo Science & Technology Bureau under Grants 2018B10063 and 2018B10064, and in part by the Department of Science and Technology of Zhejiang under Grant 2018C01058. (Corresponding author: Daofei Li.)

The authors are with the Institute of Power Machinery and Vehicular Engineering, Zhejiang University, Hangzhou 310027, China (e-mail: dfl@zju.edu.cn; jiankanhu@zju.edu.cn).

Digital Object Identifier 10.1109/LRA.2021.3101050

(Daofei Li)

(Jiankan Hu)

Abstract—Miksch *et al.*

[2].

가

가

가

가

Kuiper *et al.* [3]

가

가

가

가

가

21% 37%

(MSDV)

[4].

가

Index Terms—

I.

"

"

가

가

"

,가

가

, Salt

er *et al.*

[1].

Manuscript received April 3, 2021; accepted July 25, 2021. Date of publication July 30, 2021; date of current version August 17, 2021. This letter was recommended for publication by Associate Editor A. Pierson and Editor S. J. Guy upon evaluation of the reviewers' comments. This work was supported in part by the Ningbo Science & Technology Bureau under Grants 2018B10063 and 2018B10064, and in part by the Department of Science and Technology of Zhejiang under Grant 2018C01058. (*Corresponding author: Daofei Li.*)

The authors are with the Institute of Power Machinery and Vehicular Engineering, Zhejiang University, Hangzhou 310027, China (e-mail: dfl@zju.edu.cn; jiankanhu@zju.edu.cn).

Digital Object Identifier 10.1109/LRA.2021.3101050

in vertical direction. Here we only focus on horizontal motion control, which basically is more related to automated driving. Ukita *et al.* [5] introduce a vehicle motion control algorithm based on subjective vertical conflict (SVC) model, which can indicate the motion sickness level of passengers. The error between the sensed and the subjective vertical stimuli is used as the evaluation index of sickness rather than commonly-used acceleration or jerk. However, the SVC model is complicated and non-linear, which increases computational complexity and makes it difficult to deploy in practice. Saruchi *et al.* [6] propose a lateral control strategy that minimize roll angle of passenger head, and the SVC model is used to evaluate the effectiveness of the controller. In these two researches, only simulation is carried out, while the effectiveness has not been well validated.

On the other hand, due to its main role in automated driving algorithms, the control module is aimed to follow the planned path and velocity, i.e., a better control strategy leads to a more precise realization of the planned motion. Therefore, it is more attractive to improve the motion planning algorithm than just to optimize the control algorithm. Here we propose a new conception of motion sickness mitigation in automated driving, i.e., first to plan a desired set of vehicle motion less likely to cause car-sickness and then to precisely track it.

The contributions of this work are two-fold: (1) Motion sickness is settled in motion planning rather than control, contributing to better flexibility and compatibility in practice. (2) Frequency-shaping based planning algorithm optimizes vehicle motion in frequency domain rather than time domain. The approach is validated via both simulation and experiment.

II. MOTION PLANNING ALGORITHM

A. Algorithm Structure

Motion sickness dose value (MSDV) was introduced in ISO 2631-1:1997 standard, "Mechanical vibration and shock – Evaluation of human exposure to whole-body vibration – Part 1: General requirements." Based on experiments carried out by O'Hanlon and McCauley[7], [8], ISO 2631 argues that the frequency of acceleration stimulus has influences on motion sickness, along with the amplitude and exposure time of acceleration. In other words, motion sickness is basically a problem in frequency domain.

According to ISO 2631, MSDV is defined as

$$MSDV = \sqrt{\int_0^T [\tilde{a}(t)]^2 dt} \quad (1)$$

where \tilde{a} is the stimulus acceleration weighted by function W_f , as defined in ISO 2631-1:1997, and T is the total exposure time under such acceleration. As shown in Fig. 1, the frequency weighting function W_f works as a band pass filter and peaks at approximately 0.16 Hz, indicating that low frequency stimuli around 0.16 Hz have the greatest impact on motion sickness, while the stimuli higher than 1 Hz frequency contribute far less. [9] also suggests that 0.0315 to 0.25 Hz is a sensitive range of lateral acceleration stimuli for motion sickness.

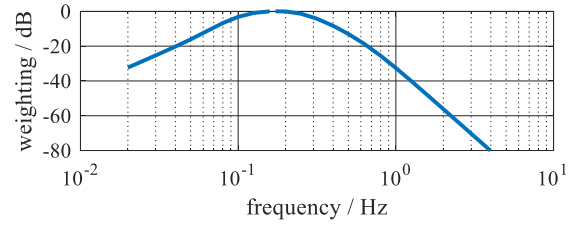


Fig. 1. Weighting curve of function W_f defined in ISO 2631-1:1997.

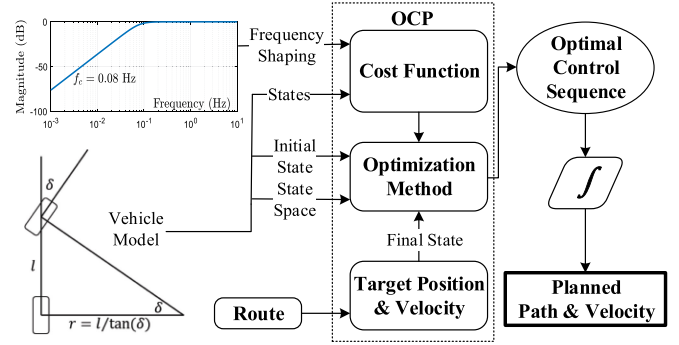


Fig. 2. Structure of motion planning algorithm with frequency domain understanding.

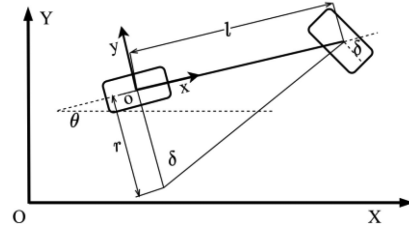


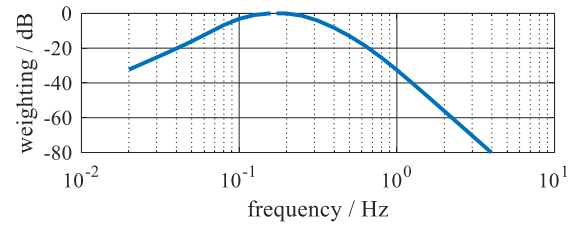
Fig. 3. Single-track vehicle kinematic model.

Based on this fact of frequency-specific sickness sensitivity, a motion planning algorithm with frequency domain understanding is proposed, as shown in Fig. 2. Motion planning is formulated as an optimal control problem (OCP), of which the cost function is defined using frequency shaping approach. Given target positions and velocity profiles from a route planner, the control sequence is obtained in OCP by minimizing the cost, and finally the planned vehicle trajectory is determined.

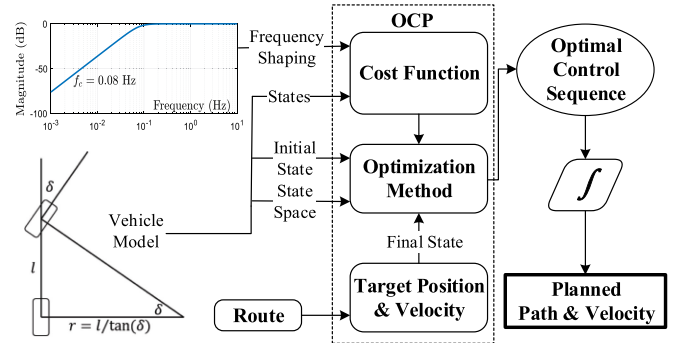
Note that in the proposed framework the real mitigation happens in motion planning rather than motion control, therefore, no special concern of motion sickness in developing motion control algorithms is needed for practical deployments, neither path following nor velocity tracking control. This is also different from previous studies of motion sickness mitigation in automated driving, e.g., motion control algorithms proposed in [5] and [6]. With only few vehicle parameters needed for the motion planning algorithm, the proposed solution is easier and more flexible to deploy in different vehicles.

B. Vehicle Model

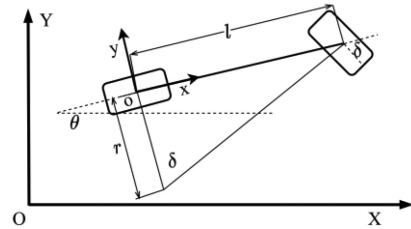
A single-track vehicle kinematic model is considered, as shown in Fig 3. The vehicle is moving in global Cartesian coordinate system XOY, and the xoy coordinate is attached to



1. ISO 2631-1:1997

 W_f 가

2.



3.

II.

A. Algorithm Structure

(MSDV) ISO 2631-1:1997 "가 - 1 : 2 가
 " O'Hanlon McCauley[7] (OCP)
 , [8]가 가 가 OCP

ISO 2631 MSDV

$$MSDV = \sqrt{\int_0^T [\tilde{a}(t)]^2 dt} \quad (1)$$

, [5] [6]

\tilde{a} ISO 2631-1:1997 가 , T 가 W_f 가

W_f , 1 가 0.16Hz 가
 0.16Hz 1Hz 가

B. Vehicle Model

25Hz가 가 . [9] 0.0315~0.3

xoy

XOY

the vehicle with x axis pointing to front and y axis pointing to left. With the center point of rear axle indicating the origin of the vehicle coordinate frame, we have

$$\dot{X} = v \cos(\theta) \quad (2)$$

$$\dot{Y} = v \sin(\theta) \quad (3)$$

$$\dot{v} = a_x \quad (4)$$

where (X, Y) is vehicle position, θ is heading angle, v is velocity and a_x is longitudinal acceleration. For yaw rate $\dot{\theta}$ and the front wheel steering angle δ , we have

$$\dot{\theta} = v \rho \quad (5)$$

$$\rho = 1/r = l/\tan(\delta) \quad (6)$$

where r is vehicle turning radius, l is wheelbase, and ρ is path curvature. Then vehicle lateral acceleration can be calculated:

$$a_y = v^2 \rho \quad (7)$$

It may be attractive to use longitudinal acceleration a_x and path curvature ρ as system inputs. However, considering the continuity of physical variables a_x and ρ , we set their derivatives with respect to time, i.e., \dot{a}_x and $\dot{\rho}$, as the inputs. Then the vehicle model can be finally described as

$$\dot{\mathbf{x}}_v = \mathbf{f}_v(\mathbf{x}_v, \mathbf{u}) \quad (8)$$

where $\mathbf{x}_v = [X, Y, v, \theta, a_x, \rho]^T$ is vehicle state vector, $\mathbf{u} = [u_1, u_2]^T = [\dot{a}_x, \dot{\rho}]^T$ is vehicle input vector.

C. Cost Function in OCP Formulation

In motion planning, a common practice is to define cost function as follows, to optimize ride comfort by minimizing the vehicle acceleration in longitudinal and lateral directions,

$$J_a = J_{ax} + J_{ay} = \int_0^{t_f} \left\{ [a_x(t)]^2 + [a_y(t)]^2 \right\} dt \quad (9)$$

where terminal time t_f indicates the end of planning horizon.

As mentioned above, acceleration in different frequency band stimulates passenger motion sickness differently. In other words, for passengers, acceleration in some frequency bands is harsher than others, so it is possible to reshape the acceleration in frequency domain to minimize the stimuli to motion sickness while keeping vehicle maneuverability. Taking $[a_x(t)]^2$ in (9) as an example, we rewrite the first cost item in the form of frequency domain using Parseval's theorem [10]:

$$J_{ax} = \int_0^{t_f} [a_x(t)]^2 dt = \int_{-\infty}^{+\infty} A_x^*(j\omega) A_x(j\omega) d\omega \quad (10)$$

where A_x is the Fourier transform of a_x and A_x^* is the complex conjugate of A_x . Clearly, in this formulation all frequencies of a_x are considered equally. Then we add a frequency-dependent weighting function $w(j\omega)$,

$$J_{ax,w} = \int_{-\infty}^{+\infty} A_x^*(j\omega) w(j\omega) A_x(j\omega) d\omega, \quad (11)$$

and decompose $w_x(j\omega)$ as follows

$$w_x(j\omega) = p^*(j\omega) p(j\omega). \quad (12)$$

Then the cost corresponding to longitudinal acceleration a_x can be rewritten in frequency domain as

$$J_{ax,w} = \int_{-\infty}^{+\infty} [A_{xw}^*(j\omega) A_{xw}(j\omega)] d\omega, \quad (13)$$

$$A_{xw}(j\omega) = p(j\omega) A_x(j\omega) \quad (14)$$

To minimize the stimuli in the most sensitive frequency band from 0.0315 to 0.25 Hz, a band-pass filter should be adopted. However, due to powertrain, braking and steering actuator limits, the vehicle control level is usually a low-pass filter system, and a commanded acceleration from motion planning is not achievable when its frequency is higher than 0.25 Hz. Therefore, to represent a cost of motion stimuli over 0.0315 Hz, here the weighting filter $p(j\omega)$ is chosen as a second order high-pass filter, i.e.,

$$p(j\omega) = (j\omega)^2 / [(j\omega)^2 + j\xi\omega_c\omega + \omega_c^2], \quad (15)$$

where $\xi = \sqrt{2}$ is the damping factor, $\omega_c = 2\pi f_c$, and f_c is the cut-off frequency to be refined.

By introducing new variables $z_1 \sim z_4$, we have the frequency-weighted accelerations a_{xw} and a_{yw} .

$$\begin{cases} a_{xw} = \dot{z}_1 = -\xi\omega_c z_1 - \omega_c^2 z_2 + a_x \\ \dot{z}_2 = z_1 \\ a_{yw} = \dot{z}_3 = -\xi\omega_c z_3 - \omega_c^2 z_4 + v^2 \rho \\ \dot{z}_4 = z_3 \end{cases} \quad (16)$$

To minimize the effect of a_{xw} and a_{yw} on motion sickness, the corresponding cost form should be aligned with MSDV definition. Similarly to that in ISO 2631-1:1997, for the vehicle planar motion, the MSDV due to longitudinal and lateral acceleration stimulation is calculated as

$$MSDV = \sqrt{\int_0^T \left\{ [\tilde{a}_x(t)]^2 + [\tilde{a}_y(t)]^2 \right\} dt} \quad (17)$$

where \tilde{a}_x and \tilde{a}_y are longitudinal and lateral accelerations weighted by function W_f in ISO 2631-1:1997, respectively, and T is the motion exposure time. Therefore, during the considered planning horizon $t \in [0, t_f]$, the corresponding cost for frequency-weighted accelerations a_{xw} and a_{yw} is selected as

$$J_{aw} = \int_0^{t_f} \left\{ [a_{xw}(t)]^2 + [a_{yw}(t)]^2 \right\} dt. \quad (18)$$

However, due to the high pass filter dynamics in (16), a_{xw} and a_{yw} does not converge to zero immediately after the terminal time t_f , so an extra cost J_{aw,t_f} corresponding to the unsettled a_{xw} and a_{yw} after t_f is added.

$$J_{aw,t_f} = \int_{t_f}^{+\infty} \left\{ [a_{xw}(t)]^2 + [a_{yw}(t)]^2 \right\} dt \quad (19)$$

Without loss of generality, to calculate this extra cost J_{aw,t_f} , we assume the vehicle will keep straight with a constant velocity,

x 가 y 가 .

$$\dot{X} = v \cos(\theta) \quad (2)$$

$$\dot{Y} = v \sin(\theta) \quad (3)$$

$$\dot{v} = a_x \quad (4)$$

(X,Y) , θ , v , a_x
가 . $\dot{\theta}$ δ

$$\dot{\theta} = v \rho \quad (5)$$

$$\rho = 1/r = l/\tan(\delta) \quad (6)$$

r , l , ρ
가

$$a_y = v^2 \rho \quad (7)$$

가 a_x ρ
.

ρ , \dot{a}_x $\dot{\rho}$

$$\dot{\mathbf{x}}_v = \mathbf{f}_v(\mathbf{x}_v, \mathbf{u}) \quad (8)$$

$$\mathbf{x}_v = [X, Y, v, \theta, a_x, \rho]^T, \\ \mathbf{u} = [u_1, u_2]^T = [\dot{a}_x, \dot{\rho}]^T.$$

C. Cost Function in OCP Formulation

가

$$J_a = J_{ax} + J_{ay} = \int_0^{t_f} \left\{ [a_x(t)]^2 + [a_y(t)]^2 \right\} dt \quad (9)$$

, t_f ,
가

가 , Parseval [1

0]

$$J_{ax} = \int_0^{t_f} [a_x(t)]^2 dt = \int_{-\infty}^{+\infty} A_x^*(j\omega) A_x(j\omega) d\omega \quad (10)$$

A_x a_x A_x^* A_x
.

가 $w(j\omega)$

$$J_{ax,w} = \int_{-\infty}^{+\infty} A_x^*(j\omega) w_x(j\omega) A_x(j\omega) d\omega, \quad (11)$$

$$w_x(j\omega) . \\ w_x(j\omega) = p^*(j\omega) p(j\omega). \quad (12)$$

가 a_x

$$J_{ax,w} = \int_{-\infty}^{+\infty} [A_{xw}^*(j\omega) A_{xw}(j\omega)] d\omega, \quad (13)$$

$$A_{xw}(j\omega) = p(j\omega) A_x(j\omega) \quad (14)$$

가 0.0315~0.25Hz

가 0.25Hz 가

0.0315Hz
가 $p(j\omega)$ 2

$$p(j\omega) = (j\omega)^2 / \left[(j\omega)^2 + j\xi\omega_c\omega + \omega_c^2 \right], \quad (15)$$

$$\xi = \sqrt{2}, \quad \omega_c = 2\pi f_c, \quad f_c$$

$z_1 \sim z_4$ 가 가

$$\begin{cases} a_{xw} = \dot{z}_1 = -\xi\omega_c z_1 - \omega_c^2 z_2 + a_x \\ \dot{z}_2 = z_1 \\ a_{yw} = \dot{z}_3 = -\xi\omega_c z_3 - \omega_c^2 z_4 + v^2 \rho \\ \dot{z}_4 = z_3 \end{cases} \quad (16)$$

a_{xw} a_{yw} MSDV . ISO 2631-1:

1997

가 MSDV

$$MSDV = \sqrt{\int_0^T \left\{ [\tilde{a}_x(t)]^2 + [\tilde{a}_y(t)]^2 \right\} dt} \quad (17)$$

\tilde{a}_x \tilde{a}_y ISO 2631-1:1997 W_f
가 , T
 $t \in [0, t_f]$

가 가 a_{xw} a_{yw}

$$J_{aw} = \int_0^{t_f} \left\{ [a_{xw}(t)]^2 + [a_{yw}(t)]^2 \right\} dt. \quad (18)$$

(16) a_{xw} a_{yw}
 t_f 0 , t_f
 a_{xw} a_{yw} 가 J_{aw,t_f} 가

$$J_{aw,t_f} = \int_{t_f}^{+\infty} \left\{ [a_{xw}(t)]^2 + [a_{yw}(t)]^2 \right\} dt \quad (19)$$

가 J_{aw,t_f}
가

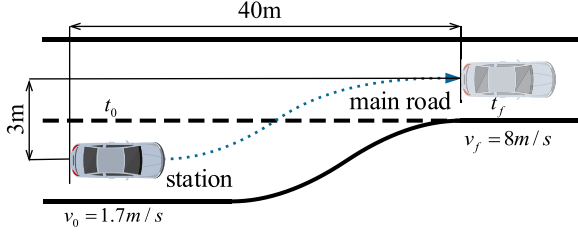


Fig. 4. Simulation scenario of "pulling-out" from a bus station.

i.e., $a_x = a_y = 0$, when $t > t_f$. Then we have

$$J_{aw,t_f} = \frac{\omega_c z_1^2(t_f)}{\xi} + \frac{\omega_c^2 z_1(t_f) z_2(t_f)}{\xi^2} + \frac{\omega_c z_3^2(t_f)}{\xi} + \frac{\omega_c^2 z_3(t_f) z_4(t_f)}{\xi^2} \quad (20)$$

Two cost items are added to minimize control inputs, i.e.,

$$J_{u_i} = \int_0^{t_f} [u_i(t)]^2 dt, \quad i = 1, 2 \quad (21)$$

Finally, an optimal control problem is established to find the best control inputs, i.e.,

$$\min_{\mathbf{u}} J = w_1 J_{aw} + w_1 J_{aw,t_f} + w_2 J_{u_1} + w_3 J_{u_2} \quad (22a)$$

$$\text{s.t. } \dot{\mathbf{x}} = \mathbf{f}(\mathbf{x}, \mathbf{u}), \mathbf{x}(0) = \mathbf{x}_0, \mathbf{g}(\mathbf{x}(t_f)) = \mathbf{0} \quad (22b)$$

where w_1, w_2, w_3 are weighting factors, $\mathbf{x} = [\mathbf{x}_v^T \ z_1 \ z_2 \ z_3 \ z_4]^T$ is the system state by combining (8) and (16), and $\mathbf{g}(\mathbf{x}(t_f)) = \mathbf{0}$ is the terminal constraint according to target position and velocity. Here the optimal control problem is handled with the classical variational method and the derived boundary value problem is solved via the MATLAB function `bvp5c` [11].

Equality constraint (22b) has already included the dynamical constraints, initial and terminal constraints. With penalty and augmented Lagrangian methods, the cost function can be further extended to include other considerations. For example, collision constraints in inequality form can be penalized as a cost based on the vehicle distance to an obstacle. For more complex forms of costs and constraints, Pontryagin's minimum principle or Dynamic Programming approaches can be used to solve the OCP.

III. PRELIMINARY VALIDATION VIA SIMULATION

A. Example Scenario for Validation

In practice, the proposed planning algorithm runs real-time, given updated initial and final conditions in the OCP framework. To simulate typical operating situations of autonomous ride-hailing vehicles, e.g., RoboBus, a picking-up-passengers maneuver, i.e., "pulling-out" from bus stations, is selected as our validation scenario, as shown in Fig. 4.

The vehicle accelerates from the station after passengers getting onboard and merges into the main road traffic flow. Since most engine-driven vehicles with automatic transmission, including our experiment vehicle, usually have a "creep" mode, it is difficult to precisely control the acceleration of the vehicle

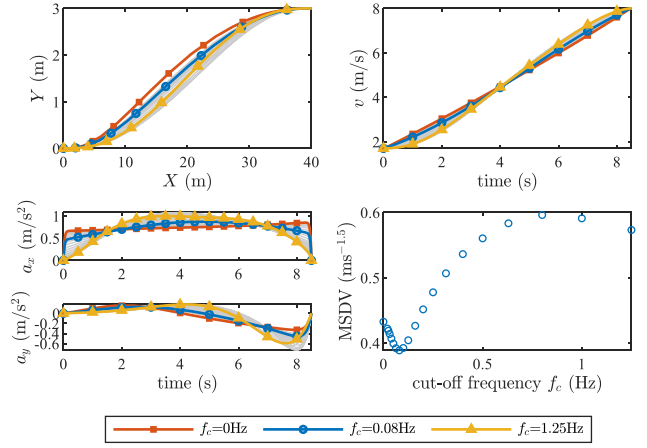
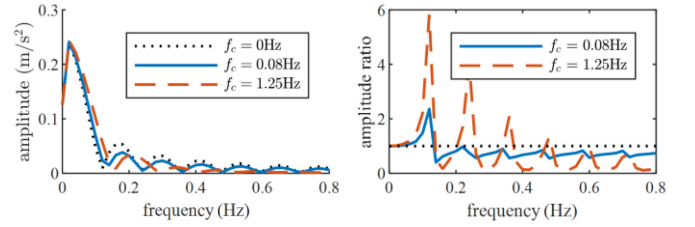
Fig. 5. Planning results with cut-off frequencies $f_c \in [0, 1.25]$ Hz.

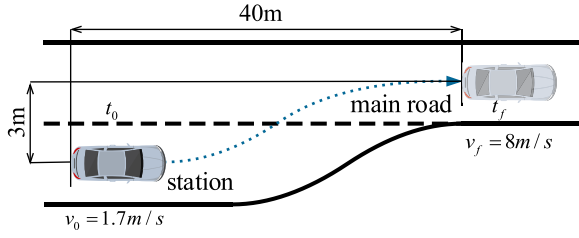
Fig. 6. FFT results of longitudinal acceleration with three cut-off frequencies (left), the ratio of amplitude at different frequencies between frequency shaping approach and non-shaping approach (right).

in extremely low speeds. Therefore, in our simulation and later real vehicle implementation, the initial speed is not 0 but 1.7 m/s, which is also the creep speed of our experiment vehicle. To simulate congested urban driving conditions, which are particularly in favor of motion sickness, the speed of the main road traffic is assumed to be about 30 km/h. To further facilitate our later on-campus experiments, v_f is determined to be 8 m/s. According to the actual setting standard in Hangzhou city, the geometry parameters of the bus station are selected with a lateral offset of 3 m and a longitudinal offset of 40 m.

B. Cut-off Frequency Selection

By setting initial time $t_0 = 0$ s, terminal time $t_f = 8.5$ s and weightings as $w_1 = 1, w_2 = 0.001, w_3 = 100$, the path and velocity planning results using different cut-off frequencies within $f_c \in [0, 1.25]$ Hz, are compared in Fig. 5. The shapes of longitudinal and lateral accelerations are different when different cut-off frequencies are chosen. Note that, according to (15), $p(j\omega) = 1$ when $f_c = 0$ Hz, which means the unshaped cost function in (9) is used. This special case can also work as an algorithm benchmark not considering frequency shaping.

For simulation, we assume the vehicle is equipped with ideal control algorithm that maintains the vehicle on planned path at planned velocity without any error. Fig. 5 presents the MSDV of vehicle planning with various cut-off frequencies, and Fig. 6 shows the FFT (Fast Fourier Transform) results of a_x with different cut-off frequencies f_c as 0, 0.08 and 1.25 Hz.



4.

i.e., $a_x = a_y = 0$, when $t > t_f$. Then we have

$$J_{aw,t_f} = \frac{\omega_c z_1^2(t_f)}{\xi} + \frac{\omega_c^2 z_1(t_f) z_2(t_f)}{\xi^2} + \frac{\omega_c z_3^2(t_f)}{\xi} + \frac{\omega_c^2 z_3(t_f) z_4(t_f)}{\xi^2} \quad (20)$$

가

가

$$J_{u_i} = \int_0^{t_f} [u_i(t)]^2 dt, \quad i = 1, 2 \quad (21)$$

가

$$\min_{\mathbf{u}} J = w_1 J_{aw} + w_1 J_{aw,t_f} + w_2 J_{u_1} + w_3 J_{u_2} \quad (22a)$$

$$\text{s.t. } \dot{\mathbf{x}} = \mathbf{f}(\mathbf{x}, \mathbf{u}), \mathbf{x}(0) = \mathbf{x}_0, \mathbf{g}(\mathbf{x}(t_f)) = \mathbf{0} \quad (22b)$$

$$\mathbf{J}^T \quad (8) \quad (16) \quad w_1, w_2, w_3 \quad \text{가} \quad \mathbf{x} = [\mathbf{x}_v^T \quad z_1 \quad z_2 \quad z_3 \quad z_4]^T, \quad \mathbf{g}(\mathbf{x}(t_f)) = \mathbf{0}$$

MATLAB bvp5 c [11]

(22b)

Pontryagin

OCP

III.

A. Example Scenario for Validation

OCP

(: RoboBus)

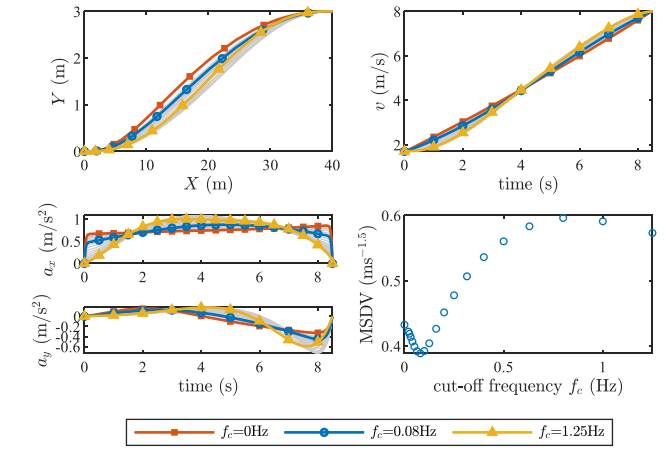
4

가

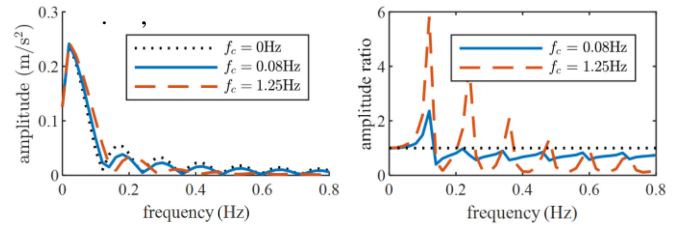
가

가

가



5.

 $f_c \in [0, 1.25] \text{ Hz}$ 

6.3

가

FFT (),

(

).

0 1.7m/s ,

30km/h 가

 $v_f = 8 \text{ m/s}$

3m,

40m

B. Cut-off Frequency Selection

$$\begin{aligned} t_0 &= 0, & t_f &= 8.5 \\ \text{가} & w_1 = 1, w_2 = 0.001, w_3 = 100 & f_c &\in [0, 1.25] \text{ Hz} \end{aligned}$$

가

5)

 $f_c = 0 \text{ Hz}$

가

가

$$p(j\omega) = 1 \quad (9)$$

.(1

MSDV

5

6 0,0

.08 1.25Hz

 f_c a_x

FFT(

In Fig. 5, the time consumption $t_f - t_0$, initial and terminal speeds are set equal for all cases, meaning that the time efficiency is the same. Since the frequency weighting function in planning uses a high-pass filter, with which the cost function in OCP can suppress the energy of acceleration above the cut-off frequency (usually over 0.0315 Hz). Results show that as f_c increases, MSDV has a minimum at 0.08 Hz. According to Fig. 1, the acceleration of frequency from 0.08 Hz to 0.315 Hz has a higher weight than others. When the cut-off frequency is less than 0.08 Hz, the acceleration energy in the high-weight frequency band decreases more and more, as the cut-off frequency rises. However, when the cut-off frequency is greater than 0.08 Hz, the acceleration energy in the high-weight frequency band starts to be excluded from the cost function as the cut-off frequency rises, resulting in increasing of MSDV.

This is further supported by the FFT results in Fig. 6. The frequency shaping approach does work in suppressing the amplitude of acceleration in the sensitive frequency band. When f_c is 0.08 Hz, the acceleration under 0.12 Hz is not suppressed, while the acceleration at the frequency band that contributes more for MSDV is weakened. When $f_c = 1.25$ Hz, acceleration at frequency band under 0.5 Hz is lifted up, covering the frequency band of 0.08 Hz to 0.315 Hz that contributes more for MSDV, and this is why MSDV gets even higher than that of non-frequency-shaping approach ($f_c = 0$ Hz). For the example implementation, we choose $f_c = 0.08$ Hz and its Bode plot is also shown in Fig. 2.

C. Comparison With Benchmark Algorithm

Motion planning based on polynomial curve fitting is widely used, in which the path and velocity of the vehicle are described as a polynomial function versus time, and the parameter of the function is defined in two steps. Firstly, the initial state which indicates the initial position and velocity, and the first derivate at initial state, which indicates the acceleration, are equal to the vehicle state at the time point the planning starts. And then the other parameters are calculated with optimization method to meet the planning target, including the destination constraints and some other requirements like comfort.

A polynomial-curve based planning approach by [12] is used as the benchmark algorithm. The vehicle is described as a lumped mass, and the velocity v and yaw rate ω_r are used to indicate the motion of the vehicle. As long as the function of $v(t)$ and $\omega_r(t)$ are chosen, the motion or the trajectory of the vehicle is determined. In this study, a 5th-order polynomial function is used to describe velocity $v(t)$ and a 3rd-order polynomial function is used to describe yaw rate $\omega_r(t)$:

$$v(t) = a_0 + a_1t + a_2t^2 + a_3t^3 + a_4t^4 + a_5t^5 \quad (23)$$

$$\omega_r(t) = b_0 + b_1t + b_2t^2 + b_3t^3 \quad (24)$$

The optimal planning, i.e., a_i^* ($i = 0, \dots, 5$) and b_j^* ($j = 0, \dots, 3$) for (23) and (24), is obtained by minimizing the following cost, subject to (22b). Here Newton method is used

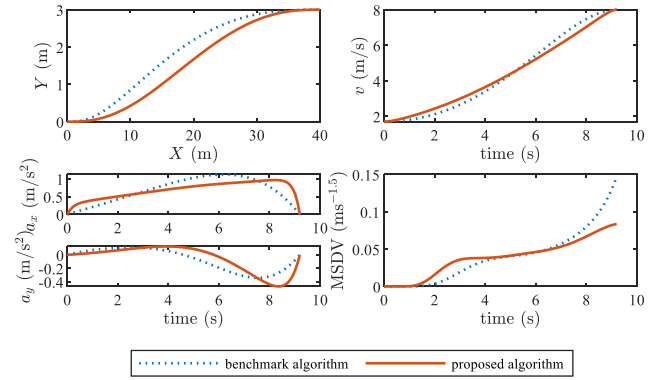


Fig. 7. Simulation results of proposed and benchmark algorithms.

to solve the optimization problem.

$$\min_{a_i, b_j} \int_0^{t_f} \left\{ [a_x(t)]^2 + [a_y(t)]^2 + 5 * [\dot{a}_x(t)]^2 \right\} dt \quad (25)$$

Fig. 7 shows the results of both algorithms, as defined in (22) and (25), respectively. The path and the velocity of the proposed algorithm is closer to a straight line, which means the average acceleration of the proposed algorithm is smaller than the benchmark. The RMS (root-mean-square) of longitudinal acceleration of the proposed algorithm (0.7505 m/s^2) is smaller than the benchmark algorithm (0.8021 m/s^2), and so is the lateral acceleration (0.1925 m/s^2 vs 0.1933 m/s^2). Thus, from the perspective of acceleration, the ride comfort of the proposed algorithm is slightly better than that of the benchmark.

As shown in Fig. 7, the peak gradient of acceleration of the proposed algorithm is much bigger than the benchmark. So if considering only motion jerk, the benchmark algorithm is actually better, thanks to its explicit inclusion of jerk in cost function (27). However, if considering motion sickness, the MSDV values with the benchmark and proposed algorithms are $0.4974 \text{ ms}^{-1.5}$ and $0.38855 \text{ ms}^{-1.5}$, respectively. It means the proposed algorithm can provide significant mitigation effect (21.89%) of motion sickness, assuming there is ideal control to realize the planned path and velocity without any error.

IV. VALIDATION VIA REAL VEHICLE EXPERIMENT

The experiment is conducted in an automated driving SUV, with the software structure shown in Fig. 8. Firstly, a point-cloud map of the experiment site is established. Secondly, the localization can be realized by mapping the lidar signals and the point-cloud map, with the correction of the GNSS signals. An EKF state estimator is needed as the updating rate of the localization is too low (10 Hz). Finally, the MPC path-follower from Autware.AI [13] is selected and tuned to realize path following via steering. A simple velocity tracking algorithm using feed-forward and feed-back control is developed. The planned longitudinal acceleration is first mapped to the feed-forward target acceleration by the longitudinal vehicle model, and then regulated with a proportional controller in the feed-back part.

Trajectory shown in Fig. 7 is tracked in the experiment and the motion control results are shown in Fig. 9. The tracking

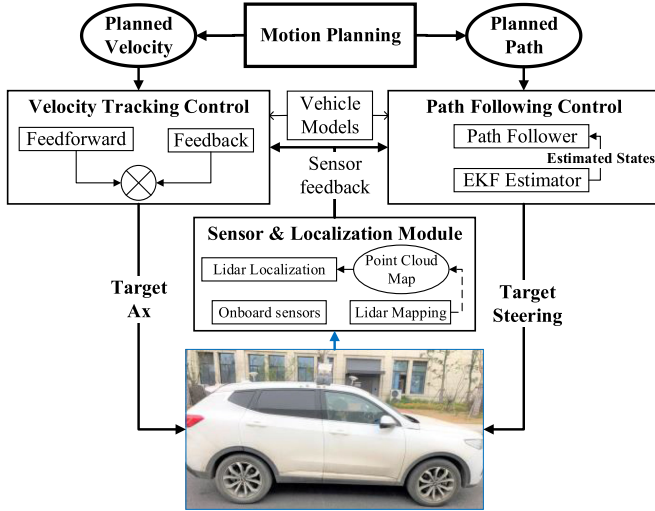


Fig. 8. Experiment vehicle and its software algorithm structure.

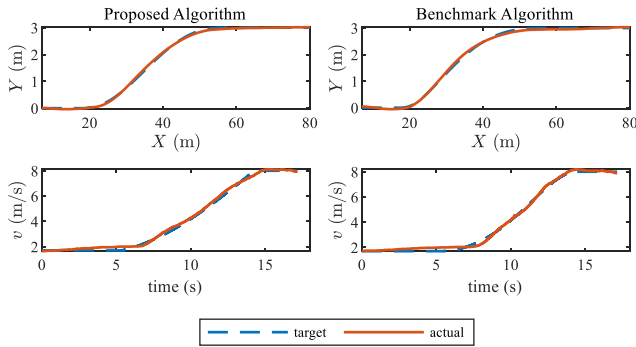


Fig. 9. Path and speed following results of both algorithms.

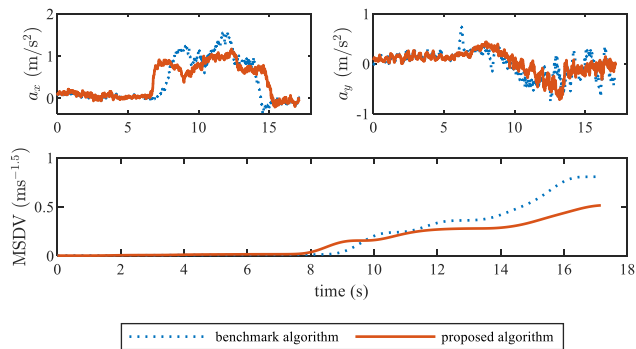


Fig. 10. Acceleration stimuli and MSDV of both algorithms.

errors are similarly small when the vehicle follows the two trajectories from the two algorithms. Vehicle accelerations, a_x and a_y , and MSDV are shown in Fig. 10. The MSDV values with the benchmark and proposed algorithms are $0.81 \text{ ms}^{-1.5}$ and $0.51 \text{ ms}^{-1.5}$, respectively, indicating 37% reduction.

As its definition indicates, MSDV works in a fashion of accumulating sickness doses, so if a RoboBus trip repeats N times of the example pulling-out motion, it will accumulate the above MSDV values to \sqrt{N} times. There is no doubt that different passengers suffer from motion sickness in different ways, and unfortunately there is not yet any recommended thresholds

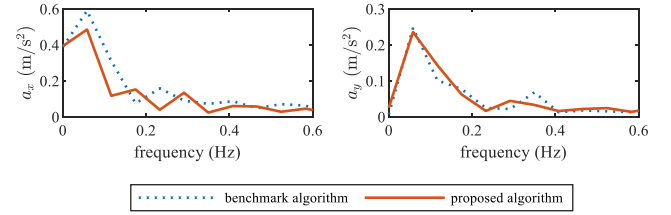


Fig. 11. FFT analysis on the acceleration stimuli of both algorithms.

of MSDV for ride comfort evaluation. The common practice in industries relies heavily on human subjective evaluation of motion comfort for final validation, while MSDV is suitable for objective evaluation. According to ISO 2631-1:1997, MSDV is positively related to Motion Sickness Incidence (MSI), which is defined as the percentage of passengers who may vomit when exposed to such motion stimuli. Therefore, the MSDV reduction in Fig. 10 implies that the percentage of passengers who may potentially suffer from motion sickness with the proposed algorithm is 37% less than that with the benchmark algorithm.

FFT is further carried out for the stimuli analysis, as shown in Fig. 11. The amplitude distribution at different frequency bands of lateral acceleration is generally similar for the two algorithms, while for longitudinal acceleration, there is a big difference at the sensitive band below 0.2 Hz. FFT results are in line with the MSDV reduction performances, and prove that the frequency shaping method does work in the example scenario.

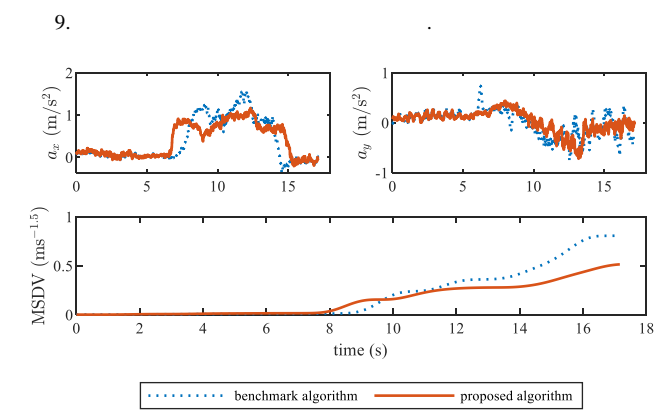
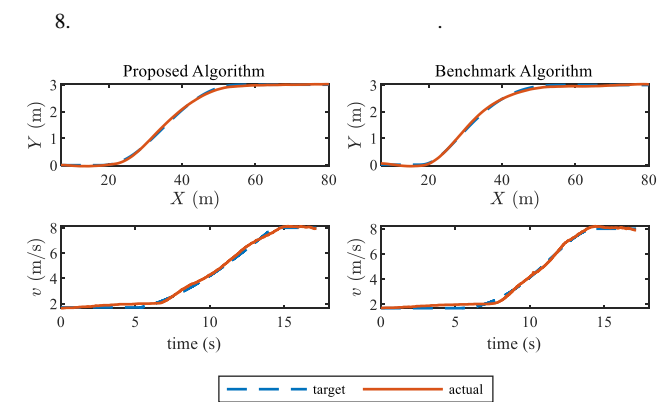
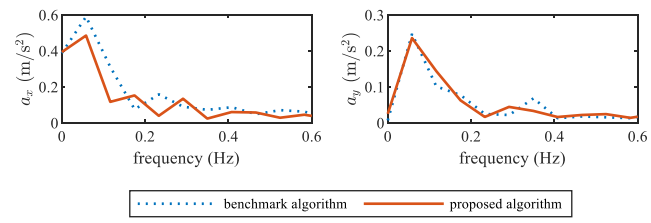
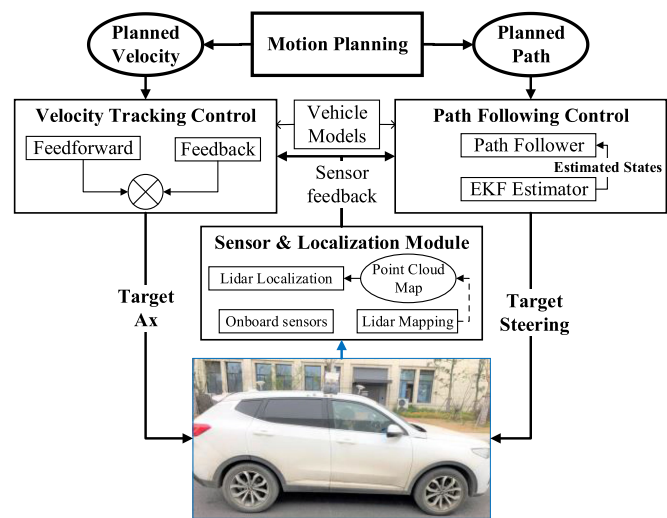
V. CONCLUSION

Motion sickness in road transportation is basically a problem in frequency domain. Conventionally, it is treated as the accumulated consequence of motion stimuli, and then solved in vehicle motion control by minimizing acceleration and jerk. We propose a new methodology of mitigating motion sickness in automated vehicles, i.e., by settling car-sickness issues earlier in motion planning via frequency-shaping approach. Real vehicle experiment indicates that the percentage of sickness mitigation effect can be as high as 37%. The proposed methodology of motion sickness mitigation may be considered a promising direction in automated driving development.

For demonstration we focus on the ride comfort improvements and the example OCP is solved using the variational method. To implement the proposed approach, more complex constraints and objectives should be handled with more advanced OCP solving methods. For future work, passenger-in-the-loop experiments, including simulator and real vehicle tests, are needed to further validate the motion sickness mitigation effectiveness of the proposed algorithm.

REFERENCES

- [1] S. Salter, C. Diels, P. Herriotts, S. Kanarachos, and D. Thake, "Motion sickness in automated vehicles with forward and rearward facing seating orientations," *Appl. Ergon.*, vol. 78, pp. 54–61, Jul. 2019, [Online]. Available: <https://doi.org/10.1016/j.apergo.2019.02.001>
- [2] M. Miksch, M. Steiner, M. Miksch, and A. Meschtscherjakov, "Motion Sickness Prevention System (MSPS): Reading between the Lines," *Ann Arbor, MI, USA*, 2016, pp. 147–152. [Online]. Available: <https://doi.org/10.1145/3004323.3004340>



10. 가 MSDV.

가 a_x a_y , MSDV가 10

MSDV $0.81\text{ms}^{-1.5}$ $0.51\text{ms}^{-1.5}$ 37%

MSDV

RoboBus

MSDV \sqrt{N}

N

11. 가 FFT .

가 MSDV.

가 . IS

O 2631-1:1997 MSDV

(MSI) 가 .

10 MSDV

37%

11 . FFT가 가

가 0.2Hz

가 . FFT MSDV

V.

가

37%

OCP

OCP

[1] S. Salter, C. Diels, P. Herriotts, S. Kanarachos, D. Thake, " ", *Appl. Ergon*, vol. 78, pp. 54 – 61, 2019 7 , []. 가 : <https://doi.org/10.1016/j.apergo.2019.02.001> [2] M. Miksch, M. Steiner, M. Miksch, A. Meschtsch erjakov, "Motion Sickness Prevention System (MSPS): Reading between the Lines," 2016, pp. 147 – 152. []. 가 : <https://doi.org/10.1145/3004323.3004340>

- [3] O. X. Kuiper, J. E. Bos, E. A. Schmidt, C. Diels, and S. Wolter, "Knowing what's coming: Unpredictable motion causes more motion sickness," *Hum Factors*, pp. 001872081987613, Oct. 2019, [Online]. Available: <https://doi.org/10.1177/0018720819876139>
- [4] O. X. Kuiper, J. E. Bos, C. Diels, and E. A. Schmidt, "Knowing what's coming: Anticipatory audio cues can mitigate motion sickness," *Appl Ergon*, vol. 85, pp. 103068, May 2020, [Online]. Available: <https://doi.org/10.1016/j.apergo.2020.103068>
- [5] R. Ukita, Y. Okafuji, and T. Wada, "A simulation study on lane-change control of automated vehicles to reduce motion sickness based on a computational mode," in *IEEE Int. Conf. Syst., Man, Cybern. (SMC)*, Oct. 2020, pp. 1745–1750. [Online]. Available: <https://doi.org/10.1109/SMC42975.2020.9283021>
- [6] S. 'A. Saruchi *et al.*, "Lateral control strategy based on head movement responses for motion sickness mitigation in autonomous vehicle," *J. Braz. Soc. Mech. Sci. Eng.*, vol. 42, no. 5, pp. 223, Apr. 2020, [Online]. Available: <https://doi.org/10.1007/s40430-020-02305-6>
- [7] J. F. O'Hanlon and M. E. McCauley, "Motion sickness incidence as a function of the frequency and acceleration of vertical sinusoidal motion," *Aerosp Med.*, vol. 45, no. 4, pp. 366–369, Apr. 1974.
- [8] M. McCauley, J. Royal, C. Wylie, J. O'Hanlon, and R. Mackie, "Motion sickness incidence: Exploratory studies of habituation, pitch and roll, and the refinement of a mathematical model," *US NAVY, Santa Barbara Res. Park, Goleta, CA*, Apr. 1976.
- [9] B. E. Donohew and M. J. Griffin, "Motion sickness: Effect of the frequency of lateral oscillation," *Aviat Space Envir Md*, vol. 75, no. 8, pp. 649–656, 2004.
- [10] N. K. Gupta, "Frequency-shaped cost functionals – extension of linear-quadratic-Gaussian design methods," *J. Guid. Control*, vol. 3, no. 6, pp. 529–535, 1980, [Online]. Available: <https://doi.org/10.2514/3.19722>
- [11] J. Kierzenka and L. F. Shampine, "A BVP solver that controls residual and error," *J. Numer. Anal. Ind. Appl. Math.*, vol. 3, no. 1/2, pp. 27–41, 2008.
- [12] T. M. Howard and A. Kelly, "Optimal rough terrain trajectory generation for wheeled mobile robots," *Ind Robot*, vol. 26, no. 2, pp. 141–166, Feb. 2007, [Online]. Available: <https://doi.org/10.1177/0278364906075328>
- [13] S. Kato, E. Takeuchi, Y. Ishiguro, Y. Ninomiya, K. Takeda, and T. Hamada, "An open approach to autonomous vehicles," *IEEE Micro*, vol. 35, no. 6, pp. 60–68, Nov. 2015, [Online]. Available: <https://doi.org/10.1109/MM.2015.133>

- [3] O. X. Kuiper, J. E. Bos, E. A. Schmidt, C. Diels, and S. Wolter, "Knowing what's coming: Unpredictable motion causes more motion sickness," *Hum Factors*, pp. 001872081987613, 2019, [10]. [11] : <https://doi.org/10.1177/0018720819876139> [4] O. X. Kuiper, J. E. Bos, C. Diels, and E. A. Schmidt, "Knowing what's coming: Anticipatory audio cues can mitigate motion sickness," *Appl Ergon*, vol. 85, pp. 103068, 2020, [12]. [13] : <https://doi.org/10.1016/j.apergo.2020.103068> [5] R. Ukita, Y. Okafuji, T. Wada, "Motion sickness during virtual reality," *IEEE Int. Conf. Syst., Man, Cybern. (SMC)*, 2020, [14], 1745-1750. [15] : <https://doi.org/10.1109/SMC42975.2020.9283021> [6] S. 'A. Saruchi et al., "Motion sickness during virtual reality," *J. Braz. Soc. Mech. Sci. Eng.*, 42, [16], 5, 223-230, 2020, [17]. [18] : <https://doi.org/10.1007/s40430-020-02305-6> [7] J. F. O'Hanlon, M. E. McCauley, "Motion sickness during virtual reality," *Aerospace Med.*, vol. 45, no. 4, pp. 366-369, 1974, [19].
- [8] M. McCauley, J. Royal, C. Wylie, J. O'Hanlon, R. Mackie, "Motion sickness during virtual reality," *US NAVY, Santa Barbara Res. Park*, [20], 1976, [21]. [22] [9] B. E. Donohew, M. J. Griffin, "Motion sickness during virtual reality," *Aviat Space Envir Md*, 75, [23], 8, 649-656, 2004. [24] [10] N. K. Gupta, "Motion sickness during virtual reality," *J. Guid. Control*, 3, [25], 6, 529-535, 1980, [26]. [27] : <https://doi.org/10.2514/3.19722> [11] J. Kierzenka, L. F. Shampine, "Motion sickness during virtual reality," *J. Numer. Anal. Ind. Appl. Math.*, vol. 3, no. 1/2, pp. 27-41, 2008. [12] T. M. Howard, A. Kelly, "Motion sickness during virtual reality," *Ind Robot*, vol. 26, no. 2, pp. 141-166, 2007, [28]. [29] : <https://doi.org/10.1177/0278364906075328> [13] S. Kato, E. Takeuchi, Y. Ishiguro, Y. Ninomiya, K. Takeda, T. Hamada, "Motion sickness during virtual reality," *IEEE Micro*, vol. 35, no. 6, pp. 60-68, 2015, [30]. [31] : <https://doi.org/10.1109/M> M. 2015.133